

# A Secondary Al–CO<sub>2</sub> Battery Enabled by Aluminum Iodide as a Homogeneous Redox Mediator

Christopher Fetrow, Cameron Carugati, Xingwen Yu, Xiao-Dong Zhou,\* and Shuya Wei\*

Cite This: *ACS Appl. Mater. Interfaces* 2023, 15, 12908–12914

Read Online

ACCESS |



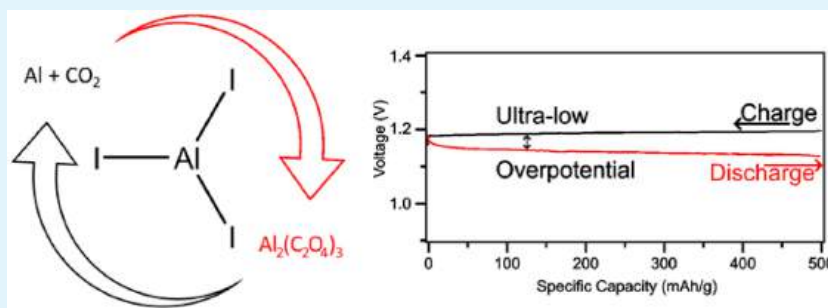
Metrics &amp; More



Article Recommendations



Supporting Information



**ABSTRACT:** As an emerging energy storage concept, Al–CO<sub>2</sub> batteries have not yet been demonstrated as a rechargeable system that can deliver a high discharge voltage and a high capacity. In this work, we present a homogeneous redox mediator to access a rechargeable Al–CO<sub>2</sub> battery with an ultralow overpotential of 0.05 V. In addition, the resulting rechargeable Al–CO<sub>2</sub> cell can maintain a high discharge voltage of 1.12 V and delivers a high capacity of 9394 mAh/g<sub>carbon</sub>. Nuclear magnetic resonance (NMR) analysis indicates that the discharge product is aluminum oxalate which can facilitate the reversible operation of Al–CO<sub>2</sub> batteries. The rechargeable Al–CO<sub>2</sub> battery system demonstrated here holds great promise as a low-cost and high-energy alternative for future grid energy storage applications. Meanwhile, the Al–CO<sub>2</sub> battery system could facilitate capture and concentration of atmospheric CO<sub>2</sub>, ultimately benefiting both the energy and environmental sectors of society.

**KEYWORDS:** Al–CO<sub>2</sub> battery, homogeneous catalyst, redox mediator, Al NMR, electrolyte additive

Metal–CO<sub>2</sub> batteries are emerging as a promising alternative power system to the prevailing lithium-ion batteries for both electric vehicle and smart grids.<sup>1,2</sup> Introducing a gaseous cathodic conversion half-reaction allows a battery to achieve a much higher specific energy density, reaching close to the practical energy density of gasoline in the ideal case.<sup>3</sup> This target is particularly important because a battery with comparable energy density to gasoline could replace combustion in most vehicles. The gas chosen for the cathodic half-reaction can be oxygen or carbon dioxide. Carbon dioxide is commonly chosen due to better applicability to in-air batteries and due to interest in electrochemical carbon capture providing another application of the metal–CO<sub>2</sub> battery.<sup>4</sup> Among the various types of metal–CO<sub>2</sub> systems demonstrated over the past decades, Li–CO<sub>2</sub> batteries have been most studied. However, metal–CO<sub>2</sub> batteries based on other metal anodes, such as Na, Mg, Al, etc., are of more interest for reducing the cost and improving safety.<sup>4</sup> Specifically, a rechargeable metal–CO<sub>2</sub> battery based on aluminum metal anode is economically advantageous considering cost-effectiveness, manufacturability, and safety handling. Furthermore, aluminum (Al) metal involves a three-electron reaction and possesses low molecular weight, which can provide an excellent gravimetric and volumetric capacity of

2980 mAh/g and 8040 mAh/cm<sup>3</sup>, comparable to the metal with the highest capacity, lithium (3860 mAh/g and 2060 mAh/cm<sup>3</sup>).<sup>5,6</sup> Aluminum anodes also have the distinct advantage of dendrite-free stripping/plating in chloraluminum electrolytes.<sup>5,7</sup> These characteristics alongside aluminum's high abundance make it a good choice as an anode for a metal–CO<sub>2</sub> battery. However, the demonstration of an effective rechargeable Al–CO<sub>2</sub> battery still poses significant challenges so far.

Sadat and Archer in 2016 designed a primary Al–CO<sub>2</sub>/O<sub>2</sub> battery in which the reduction of CO<sub>2</sub> is mediated by the introduction of 20% oxygen in the gas feed.<sup>8</sup> The battery was constructed with an aluminum metal anode, an ionic liquid electrolyte, and a nanostructured carbon cathode. The battery delivered a discharge plateau around 1.4 V with a discharge rate of 70 mA/g<sub>carbon</sub> to a final discharge capacity of 13000 mAh/g<sub>carbon</sub>. By using X-ray photoelectron spectroscopy

Received: October 11, 2022

Accepted: February 23, 2023

Published: March 3, 2023



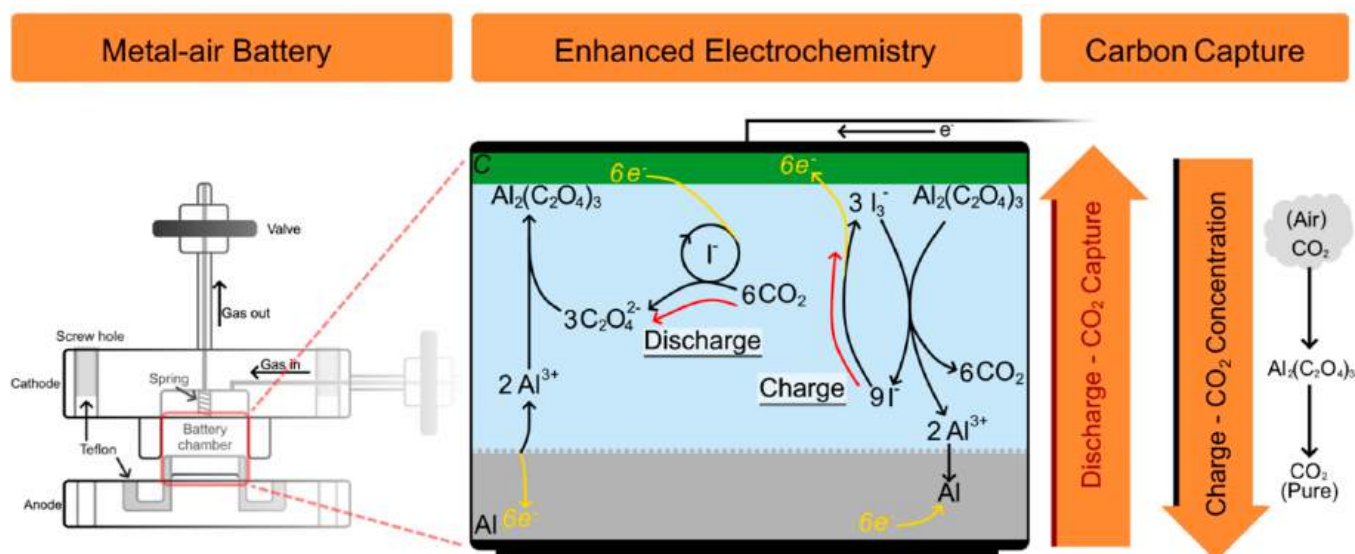


**Figure 1.** Schematic showing battery design, proposed mechanism, and possible utilization of the Al–CO<sub>2</sub> battery for carbon capture and concentration.

(XPS), the authors identified the discharge product to be aluminum oxalate. However, no decomposition of the discharge product upon battery recharging was observed, making it a primary battery. Later on, Ma et al. in 2018 demonstrated an Al–CO<sub>2</sub> battery that could be recharged using a palladium-coated nanoporous gold cathode as a catalyst.<sup>9</sup> The battery showed a discharge plateau near 0.627 V and a charge overpotential of 0.108 V, indicating a significantly altered electrochemistry compared to the previous primary battery demonstrated by Sadat and Archer. The discharge product was identified to be aluminum carbonate using X-ray photoelectron spectroscopy, which may explain the difference in discharge voltages between the two battery configurations. However, the aluminum compounds in neither of the above-discussed Al–CO<sub>2</sub> systems are well investigated until now, and there is no thermodynamic data readily available. Therefore, the exact causes for the differences in electrochemical behavior in the two Al–CO<sub>2</sub> systems remain unclear.<sup>10</sup>

To demonstrate a rechargeable Al–CO<sub>2</sub> battery with an acceptably high discharge voltage and a high specific capacity, alternative strategies are to be applied to the battery system. Homogeneous redox mediators have been previously used in Li–O<sub>2</sub> batteries as redox mediators, where during the charging process, the redox mediator is oxidized to form a reactive intermediate species that can chemically decompose the discharge product.<sup>11,12</sup> Because the discharge product of the Li–O<sub>2</sub> battery is a relatively stable insulator, using a homogeneous species to shuttle the charge and to facilitate decomposition of the discharge product can avoid high charge overpotentials. A notable redox mediator is the iodide species such as lithium iodide, which has been previously demonstrated in both Li–CO<sub>2</sub> and Li–O<sub>2</sub> batteries.<sup>13,14</sup> Shiga et al. in 2019 found that a layer of LiI formed on the surface of the cathode during discharge of a Li–CO<sub>2</sub> battery. The LiI layer could increase CO<sub>2</sub> affinity and thus enhanced the discharge capacity.<sup>13</sup> Earlier on, Liu et al. in 2015 found that the presence of LiI allowed the chemical conversion of LiO<sub>2</sub> to form LiOH during the discharge of a Li–O<sub>2</sub> battery operated with trace amount of water.<sup>14</sup> Both research groups confirmed that an I<sub>3</sub><sup>−</sup>

species was formed electrochemically during the charge process. The I<sub>3</sub><sup>−</sup> species could chemically enhance the degradation of discharge product to improve the reversibility of Li–CO<sub>2</sub> and Li–O<sub>2</sub> batteries.

On the basis of the success in applying a redox mediator in Li–CO<sub>2</sub> systems, we speculate that a redox mediator that can degrade the aluminum discharge product during charge is expected to enable a rechargeable Al–CO<sub>2</sub> battery with both high capacity and high energy efficiency (low overpotential). Inspired by the discussion above that the I<sub>3</sub><sup>−</sup> species could be electrochemically formed and could consequently facilitate the degrading of the stable discharge products, in this work, we introduce an aluminum iodide additive as a stable redox mediator to the electrolyte of an Al–CO<sub>2</sub> battery. The introduction of AlI<sub>3</sub> successfully enables a reversible Al–CO<sub>2</sub> battery with ultralow overpotentials across a range of current densities while maintaining both a high discharge voltage and a high capacity. The discharge products are also characterized and analyzed with NMR.

In this study, Al–CO<sub>2</sub> cells were fabricated with a mechanically polished aluminum foil anode, a Ketjen black nanostructured carbon cathode, and an aluminum chloride:1-ethyl-3-methylimidazolium chloride ionic liquid electrolyte. The cell configuration is as illustrated in Figures 1 and S1. To demonstrate the effect of the AlI<sub>3</sub> redox mediator, cells were operated with and without the AlI<sub>3</sub> additive and were discharged with and without CO<sub>2</sub>. No discharge plateau and a capacity of 3.23 mAh/g (0.00204 mAh/cm<sup>2</sup>) is observed for the battery with neither AlI<sub>3</sub> nor CO<sub>2</sub> (Figure 2a, inset), similar to the results observed by Al Sadat and Archer.<sup>8</sup> The battery with only AlI<sub>3</sub> additive also displays no discharge plateau and a capacity of 399.7 mAh/g (0.1770 mAh/cm<sup>2</sup>), while the battery containing both AlI<sub>3</sub> and CO<sub>2</sub> displays a discharge plateau at 1.12 V and a capacity of 9394 mAh/g (6.526 mAh/cm<sup>2</sup>). An additional investigation with cyclic voltammetry (CV) shows that the Al–CO<sub>2</sub> battery containing both AlI<sub>3</sub> and CO<sub>2</sub> displays a significant reduction peak at 1.15 V (Figure 2b), further indicating that the AlI<sub>3</sub> additive promotes CO<sub>2</sub> reduction during the discharge. The observed reduction peak of this battery at 1.15 V (Figure 2b) closely matches the

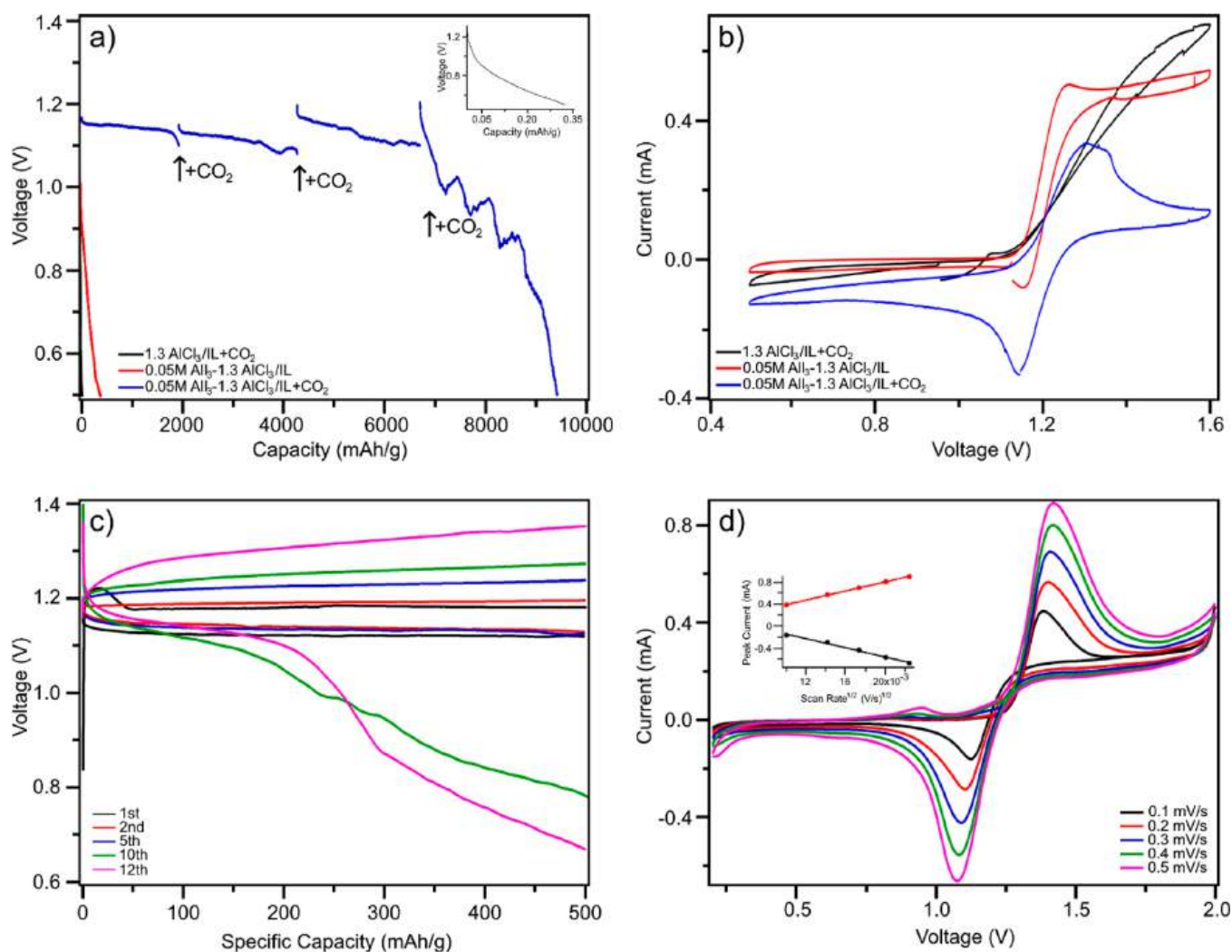


**Figure 2.** Electrochemical performance of Al–CO<sub>2</sub> batteries with and without an AlI<sub>3</sub> additive. (a) Galvanostatic discharge profile of the Al–CO<sub>2</sub> batteries at a rate of 20 mA/g<sub>carbon</sub> (mA/g). Inset: discharge of the battery without CO<sub>2</sub> or AlI<sub>3</sub> additive to show detail. (b) Cyclic voltammetry profiles of Al–CO<sub>2</sub> batteries at a scan rate of 0.1 mV/s from 0.5 to 1.6 V. The cells were prepared either with 0.05 M AlI<sub>3</sub> additive or without an additive (as indicated in the figure) and were operated either in a CO<sub>2</sub> environment or in an argon environment without CO<sub>2</sub> (as indicated in the figure). The galvanostatic discharge of the battery with AlI<sub>3</sub> and CO<sub>2</sub> was intermittently paused to add more CO<sub>2</sub> to the battery. (c) The first 12 galvanostatic cycles of an Al–CO<sub>2</sub> battery containing 0.05 M AlI<sub>3</sub> at a cycling rate of 20 mA/g. The cell was charged/discharged to a fixed capacity of 500 mAh/g. (d) Cyclic voltammetry profiles of an Al–CO<sub>2</sub> battery containing 0.05 M AlI<sub>3</sub> from 0.5 to 1.6 V at various scan rates. Inset: the relationship between the square root of scan rates and peak currents for the oxidation and reduction reactions.

observed discharge plateau voltage observed under galvanostatic cycling (Figure 2a). CV of the battery with AlI<sub>3</sub> in argon gas displays a sharpened oxidation peak (Figure 2b), showing that a reactive iodine redox species can be formed electrochemically.<sup>13</sup> CV of the battery with CO<sub>2</sub> and without AlI<sub>3</sub> shows an irreversible reaction of the CO<sub>2</sub>. Over the course of cycling with an assigned capacity of 500 mAh/g, the Al–CO<sub>2</sub> battery with the AlI<sub>3</sub> additive displays a discharge voltage plateau at 1.13 V and a charge voltage plateau at 1.17 V (Figure 2c). The first-cycle overpotential is only 0.05 V and then increases to 0.1 V after 10 cycles. The small voltage hump initially appearing in the first charge (the black line in Figure 2c) is probably due to the poor diffusion of CO<sub>2</sub> and electrolyte through the nanostructured cathode. In general, Li–CO<sub>2</sub> batteries with a heterogeneous catalyst (such as ruthenium or manganese oxide) usually exhibit an overpotential around 1 V.<sup>15–18</sup> Therefore, in comparison to those commonly used heterogeneous catalysts, the AlI<sub>3</sub> additive

shows a significantly superior capability in reducing the overpotential in Al–CO<sub>2</sub> batteries. The oxidation of solvated I<sup>−</sup> appears to be the initial step of the charge process, as direct decomposition of a solid and insulating discharge product would require a much higher overpotential.

With the CV technique, the reversibility of AlI<sub>3</sub>-mediated Al–CO<sub>2</sub> batteries is further investigated by plotting redox peak currents as a function of the square root of scan rates (Figure 2d). A completely reversible reaction is supposed to follow the Randles–Sevcik equation, in which the peak currents in CV are proportional to the square root of scan rates.<sup>19</sup> The Al–CO<sub>2</sub> battery in this study closely follows this relation (Figure 2d, inset), indicating that the oxidation charge process is the reverse of the reduction discharge reaction. A small peak at 0.95 V due to decomposition of impurities in the electrolyte can be seen in the highest scan rate sample. The reduction reaction of the cell is highly sensitive to the current rate applied, sustaining a discharge plateau to a discharge rate of 70



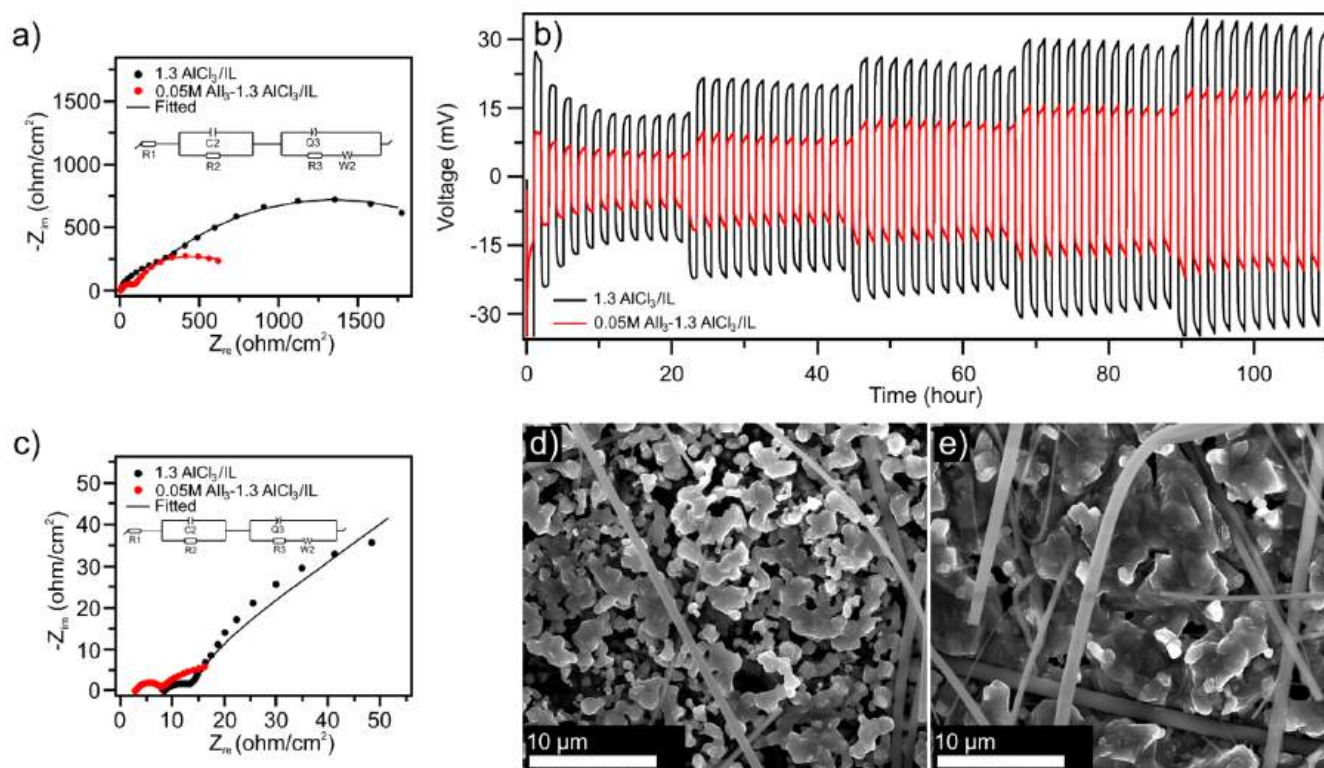


**Figure 3.** Impact of aluminum iodide additive on the electrochemical and microscopic characterizations of aluminum anode. (a) Electrochemical impedance spectroscopy of pristine symmetric Al/Al cells with and without  $\text{AlI}_3$ . (b) Stripping/plating test of symmetric Al/Al cells with and without  $\text{AlI}_3$  additive at current rates of 0.2, 0.3, 0.4, 0.5, and 1  $\text{mA}/\text{cm}^2$ . The cells were intermittently charged/discharged for 1 h in each cycle. (c) Electrochemical impedance spectroscopy of symmetric Al/Al cells with and without  $\text{AlI}_3$  after 100 h of stripping/plating at a current rate of 0.2  $\text{mA}/\text{cm}^2$ . (d, e) SEM images of aluminum anodes from Al/Al cells without and with  $\text{AlI}_3$  additive respectively after 1000 h of stripping/plating at a current rate of 0.2  $\text{mA}/\text{cm}^2$ .

$\text{mA}/\text{g}$  (Figure S2). This sensitivity has been observed previously and can be attributed to the slow kinetics of the multielectron discharge reaction mechanism of Al.<sup>8</sup> To further support the rechargeability of the Al- $\text{CO}_2$  battery, the cathodes were fabricated with added aluminum oxalate ( $\text{Al}_2(\text{C}_2\text{O}_4)_3$ ) in a 1:1 ratio to Ketjen black. As shown in Figure S3, the galvanostatic charge profile of the battery with added aluminum oxalate shows a heightened charge plateau from 1.18 to 1.3 V, which closely matches the cyclic voltammetry reduction and oxidation peak potentials (Figures 2b and S3). CV of the Al- $\text{Al}_2(\text{C}_2\text{O}_4)_3$  battery with 0.05 M  $\text{AlI}_3$  shows that after a high overpotential during the first charge cycle, the reduction and oxidation peak positions near exactly match that of an Al- $\text{CO}_2$  battery with 0.05 M  $\text{AlI}_3$  (Figure S4). These data show that the charge reaction is the decomposition of aluminum oxalate. The battery cycling for 12 cycles during galvanostatic cycling suggests that the decomposition of aluminum oxalate may not be complete (Figure 2c).

An increase in open-circuit potential of Al- $\text{CO}_2$  batteries by  $\sim 0.05$  V is observed when using electrolyte with added  $\text{AlI}_3$  (Figure 2b). To examine the effect of  $\text{AlI}_3$  on the Al anode, we constructed symmetric Al/Al cells with and without the  $\text{AlI}_3$  additive and conducted electrochemical impedance as well as stripping/plating experiments across a variety of current rates. Impedance analysis of the batteries shows that the bulk resistance is similar between the batteries with and without  $\text{AlI}_3$ , but the interfacial resistance is significantly reduced for the cell with  $\text{AlI}_3$  additive (Figure 3a). Doubling the  $\text{AlI}_3$

additive concentration to 0.1 M shows little effect on either stripping/plating overpotential or interfacial resistance, while further increasing the concentration of additive to 1.0 M negatively affects the cell performance, which might be due to the decrease in the ionic conductivity of the electrolyte (Figure S5).

The cell containing  $\text{AlI}_3$  displays a lower stripping/plating overpotential during galvanostatic cycling, with the greatest reduction in overpotential of 52.8% at the lowest current rate of 0.2  $\text{mA}/\text{cm}^2$  (Figure 3b). Impedance analysis shows that the cell with  $\text{AlI}_3$  additive maintains a lower interfacial resistance than the cell without the additive after cycling for 100 h at 0.2  $\text{mA}/\text{cm}^2$  (Figure 3c). Scanning electron microscopy (SEM) images of cell anodes after cycling for 1000 h at 0.2  $\text{mA}/\text{cm}^2$  show that cells with the  $\text{AlI}_3$  additive have a larger feature size (Figures 3d,e). The larger feature size shows that adding  $\text{AlI}_3$  facilitates smoother (homogeneous) aluminum deposition, which should also reduce parasitic reactions with the electrolyte. It is possible that the iodine-containing solid-electrolyte interphase results in a lower ion diffusion energy barrier, as has been previously calculated for sodium anodes.<sup>20</sup> Stripping/plating tests of symmetric cells with and without  $\text{AlI}_3$  show that the additive reduces and stabilizes the stripping/plating overpotential for over 1700 h at a current rate of 0.2  $\text{mA}/\text{cm}^2$  (Figure S6).

To examine the electrochemical mechanism of the Al- $\text{CO}_2$  battery, batteries were disassembled in an inert atmosphere at different stages of charge and discharge. Liquid phase samples were prepared for further characterization by rinsing the

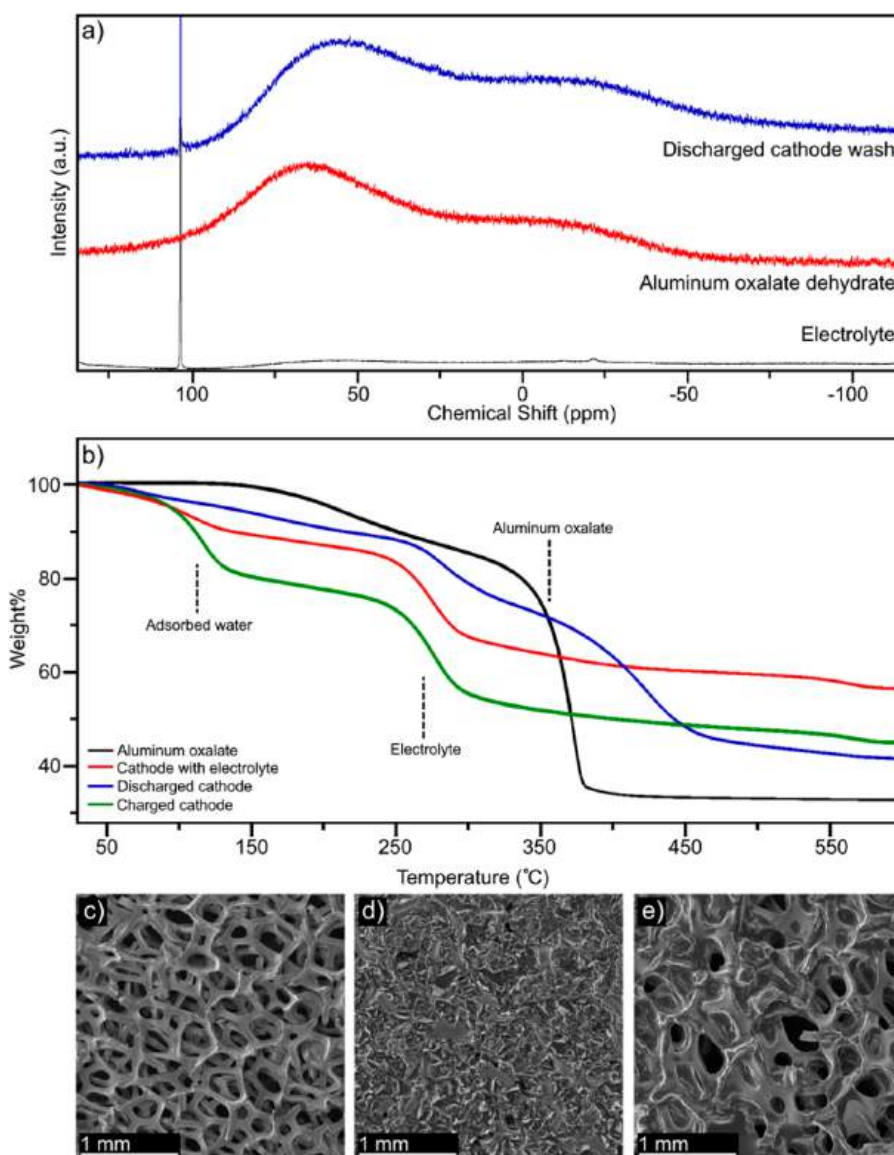


**Figure 4.** Discharge product identification for the  $\text{Al}_3$  mediated  $\text{Al}-\text{CO}_2$  batteries. (a)  $^{27}\text{Al}$  NMR spectra (78.2 MHz) of an electrolyte containing 0.05 M  $\text{Al}_3$  diluted in acetonitrile, a solution of saturated aluminum oxalate dehydrate in acetonitrile, and the collected acetonitrile used to wash the cathode of an  $\text{Al}-\text{CO}_2$  battery with  $\text{Al}_3$  after discharge. (b) TGA of the cathode of an  $\text{Al}-\text{CO}_2$  battery with  $\text{Al}_3$  after discharge, compared against an aluminum oxalate standard, a cathode wetted with the electrolyte, and a cathode from the same battery configuration after charge. Similar TGA for the battery without an  $\text{Al}_3$  additive is presented in Figure S10. (c) SEM image of pristine nickel foam. (d, e) SEM images of nickel foam cathode insets from  $\text{Al}_3$ -mediated  $\text{Al}-\text{CO}_2$  batteries after discharge (d) and after charge (e).

cathode in acetonitrile and collecting the resulting wash. The primary method used to identify the discharge product is aluminum-27 nuclear magnetic resonance ( $^{27}\text{Al}$  NMR). The 100% natural abundance and high NMR activity of the  $^{27}\text{Al}$  isotope make  $^{27}\text{Al}$  NMR practical for investigating Al-based batteries. Additionally,  $^{27}\text{Al}$  NMR has been previously used to identify the ion intercalation mechanism of the graphitic carbon nitride cathode in Al-ion batteries and the chloroaluminate speciation of novel molten salt electrolytes.<sup>7,21,22</sup> We have also applied other characterization methods to study the reaction products. However, the ionic liquid electrolyte was observed to react spontaneously in air, which can be confirmed by energy-dispersive spectroscopy (Table S1). In addition, an attempt to remove the electrolyte from the cathode was observed to remove the discharge product as well, reflected in the SEM images of a discharged cathode before and after

washing (Figure S7). Therefore,  $^{27}\text{Al}$  NMR is an ideal method to study the reaction products, as no contact with air is required. The ionic liquid electrolyte spectrum displays a single sharp peak at 103.8 ppm, which closely matches previous observation (Figure 4a).<sup>7</sup> The lack of a second, smaller peak indicates that the added  $\text{Al}_3$  dissolves to form  $\text{Al}^{3+}$  and  $\text{I}^-$  species, instead of possibly forming  $\text{AlI}_4^-$  like the known  $\text{AlCl}_3$  speciation in ionic liquid.<sup>23</sup> The electrolyte peak is clearly visible at 103.8 ppm in the discharged sample. The two broad peaks at 56.2 and  $-15.5$  ppm in the discharged sample are identified to be aluminum oxalate by comparing to an aluminum oxalate standard. The broad peaks are characteristic of a poorly solvated species with significant electronic shielding.<sup>21</sup> A small shift in peak location between the aluminum oxalate standard and the discharge product is due to the solvation effect of the electrolyte (Figure S8).

Dehydration of the aluminum oxalate standard prior to measurement was shown to not alter the sample using  $^{27}\text{Al}$  NMR (Figure S9).

Thermogravimetric analysis (TGA) was implemented to identify the discharge product as well, which further supported the results obtained from NMR. As shown in Figure 4b, aluminum oxalate decomposes under nitrogen near 350 °C. Samples also show mass loss near 100 °C from adsorbed water, and the electrolyte decomposition at 260 °C provides another mass loss peak to samples with electrolyte. The cathode of a battery with  $\text{AlI}_3$  additive discharged under  $\text{CO}_2$  also shows a significant mass loss near 350 °C due to the decomposition of aluminum oxalate. The observed decomposition temperature is above that previously reported by Al Sadat and Archer.<sup>8</sup> This is due to the difference in sample preparation. We observed aluminum oxalate to be somewhat soluble in acetonitrile (Figures 4a and S7); thus, samples were not washed prior to TGA measurement. This caused an additional mass loss peak near 250 °C due to electrolyte decomposition and an extended aluminum oxalate decomposition due to a larger particle size. Batteries with nickel foam insets between the cathode and separator were used to image the discharge product formation and degradation with SEM (Figure 4c). A thick layer of discharge product forms on the cathode after discharge (Figure 4d). After charge, the discharge product is almost completely removed (Figure 4e). There is only a thin layer of material remaining on the charged cathode that is identified to be the electrolyte by comparing to a sample of nickel foam wetted with electrolyte (Figure S11). These data strongly suggest that discharge product is forming and decomposing during battery discharge and charge, supporting the reversibility of the  $\text{Al}-\text{CO}_2$  battery from the earlier electrochemical analysis.

The introduction of  $\text{AlI}_3$  to the battery clearly enables the discharge of the  $\text{Al}-\text{CO}_2$  battery as a replacement for  $\text{O}_2$  in the previous primary  $\text{Al}-\text{CO}_2/\text{O}_2$  battery. However, unlike  $\text{O}_2$ , the  $\text{AlI}_3$  also enables the reversibility of  $\text{Al}-\text{CO}_2$  batteries. The charge mechanism could possibly follow previously identified schemes using iodine as a homogeneous redox mediator, in which the solvated iodine species (usually identified to be  $\text{I}^-$ , in some cases  $\text{I}_2$ ) is oxidized to form the reactive species  $\text{I}_3^-$ .<sup>13,14,24</sup> This reactive species then decomposes the discharge product chemically, regenerating the initial species (Figure 1). Iodine may serve to replace oxygen as a redox mediator during discharge. We do not observe direct reduction of  $\text{CO}_2$  in the absence of an additive, in agreement with previous research.<sup>25</sup> This aligns with Al Sadat and Archer's proposed mechanism in which the redox mediator is initially reduced and then acts to reduce carbon dioxide.<sup>8</sup>

In summary, we have demonstrated a rechargeable  $\text{Al}-\text{CO}_2$  battery enabled by a homogeneous redox mediator  $\text{AlI}_3$  as a proof-of-concept system capable of storing energy and concentrating carbon. While the conventional primary  $\text{Al}-\text{CO}_2/\text{O}_2$  battery is projected to result in a net reduction of  $\text{CO}_2$  emissions through carbon capture, a secondary configuration demonstrated in this research is a more powerful tool to reduce  $\text{CO}_2$  emissions due to its capability of reversible carbon concentration during normal operation before the end-of-life carbon capture. The rate capability and cycle life of the demonstrated rechargeable  $\text{Al}-\text{CO}_2$  battery still need to be improved before the technology can be used in practice. In addition to the improvement of cycling performance, our future work will include the operation of cells with an  $\text{O}_2$  associated in-air mode. From a fundamental perspective,

complete understanding of the iodine speciation in ionic liquid electrolytes will need to be rigorously studied, which is expected to allow the rational design of a high-performance rechargeable  $\text{Al}-\text{CO}_2$  battery for use in electric vehicles, grid-level energy storage, and personal electronic devices.

## ■ ASSOCIATED CONTENT

### SI Supporting Information

The Supporting Information is available free of charge at <https://pubs.acs.org/doi/10.1021/acsami.2c18323>.

Details on materials and battery fabrication, electrochemical testing equipment and parameters, material preparation methods for characterization, characterization equipment details and parameters; leak testing details of the battery holders used; predischarged cathode fabrication details; a schematic of the battery holders used (Figure S1); discharge tests of batteries at varied current rates (Figure S2); charge tests of batteries with and without  $\text{AlI}_3$  as well as with  $\text{AlI}_3$  and aluminum oxalate (Figure S3); CV of a battery with aluminum oxalate in argon compared to typical  $\text{Al}-\text{CO}_2$  battery with  $\text{AlI}_3$  (Figure S4); stripping/plating and impedance spectroscopy data of symmetric cells with increased  $\text{AlI}_3$  concentration (Figure S5); long-term stripping/plating data of symmetric cells with and without  $\text{AlI}_3$  (Figure S6); EDS data of nickel foam cathode with electrolyte wetting (Table S1); SEM images of cathodes before and after acetonitrile washing (Figure S7);  $^{27}\text{Al}$  NMR data of purchased aluminum oxalate showing effect of dehydration protocol and chemical shift due to electrolyte solvation shell (Figures S8 and S9); TGA data of battery cathodes after discharge and charge without  $\text{AlI}_3$  (Figure S10); SEM image of nickel foam inset wetted with electrolyte (Figure S11); OCV measurement of batteries with  $\text{AlI}_3$  additive exposed to atmosphere and closed to atmosphere (Figure S12) (PDF)

## ■ AUTHOR INFORMATION

### Corresponding Authors

Xiao-Dong Zhou – Department of Chemical Engineering, Institute for Materials Research and Innovations, University of Louisiana at Lafayette, Lafayette, Louisiana 70503, United States; Email: [xiao-dong.zhou@louisiana.edu](mailto:xiao-dong.zhou@louisiana.edu)

Shuya Wei – Department of Chemical and Biological Engineering, University of New Mexico, Albuquerque, New Mexico 87131, United States; [orcid.org/0000-0001-9269-1950](https://orcid.org/0000-0001-9269-1950); Email: [swei@unm.edu](mailto:swei@unm.edu)

### Authors

Christopher Fetrow – Department of Chemical and Biological Engineering, University of New Mexico, Albuquerque, New Mexico 87131, United States; [orcid.org/0000-0002-7706-901X](https://orcid.org/0000-0002-7706-901X)

Cameron Carugati – Department of Chemical and Biological Engineering, University of New Mexico, Albuquerque, New Mexico 87131, United States

Xingwen Yu – Department of Chemical Engineering, Institute for Materials Research and Innovations, University of Louisiana at Lafayette, Lafayette, Louisiana 70503, United States

Complete contact information is available at: <https://pubs.acs.org/doi/10.1021/acsami.2c18323>



## Notes

The authors declare no competing financial interest.

## ACKNOWLEDGMENTS

This work was supported by the National Science Foundation Award 2119688. S.W. acknowledges the financial support from the University of New Mexico startup fund.

## REFERENCES

- (1) Xie, Z.; Zhang, X.; Zhang, Z.; Zhou, Z. Metal–CO<sub>2</sub> Batteries on the Road: CO<sub>2</sub> from Contamination Gas to Energy Source. *Adv. Mater.* **2017**, *29* (15), 1605891.
- (2) Xie, J.; Zhou, Z.; Wang, Y. Metal–CO<sub>2</sub> Batteries at the Crossroad to Practical Energy Storage and CO<sub>2</sub> Recycle. *Adv. Funct. Mater.* **2020**, *30* (9), 1908285.
- (3) Lee, J. S.; Tai Kim, S.; Cao, R.; Choi, N. S.; Liu, M.; Lee, K. T.; Cho, J. Metal–Air Batteries with High Energy Density: Li–Air Versus Zn–Air. *Adv. Energy Mater.* **2011**, *1* (1), 34–50.
- (4) Fetrow, C. J.; Carugati, C.; Zhou, X.-D.; Wei, S. Electrochemistry of Metal–CO<sub>2</sub> Batteries: Opportunities and Challenges. *Energy Storage Materials* **2022**, *45*, 911.
- (5) Liang, Y.; Dong, H.; Aurbach, D.; Yao, Y. Current Status and Future Directions of Multivalent Metal-Ion Batteries. *Nature Energy* **2020**, *5* (9), 646–656.
- (6) Elia, G. A.; Kravchyk, K. V.; Kovalenko, M. V.; Chacón, J.; Holland, A.; Wills, R. G. An Overview and Prospective on Al and Al-Ion Battery Technologies. *J. Power Sources* **2021**, *481*, 228870.
- (7) Pang, Q.; Meng, J.; Gupta, S.; Hong, X.; Kwok, C. Y.; Zhao, J.; Jin, Y.; Xu, L.; Karahan, O.; Wang, Z.; et al. Fast-Charging Aluminium–Chalcogen Batteries Resistant to Dendritic Shorting. *Nature* **2022**, *608* (7924), 704–711.
- (8) Al Sadat, W. I.; Archer, L. A. The O<sub>2</sub>-Assisted Al/CO<sub>2</sub> Electrochemical Cell: A System for CO<sub>2</sub> Capture/Conversion and Electric Power Generation. *Sci. Adv.* **2016**, *2* (7), e1600968.
- (9) Ma, W.; Liu, X.; Li, C.; Yin, H.; Xi, W.; Liu, R.; He, G.; Zhao, X.; Luo, J.; Ding, Y. Rechargeable Al–CO<sub>2</sub> Batteries for Reversible Utilization of CO<sub>2</sub>. *Adv. Mater.* **2018**, *30* (28), 1801152.
- (10) Downs, A. J. *Chemistry of Aluminium, Gallium, Indium and Thallium*; Springer Science & Business Media: 1993.
- (11) Lacey, M. J.; Frith, J. T.; Owen, J. R. A Redox Shuttle to Facilitate Oxygen Reduction in the Lithium Air Battery. *Electrochem. Commun.* **2013**, *26*, 74–76.
- (12) Chen, Y.; Freunberger, S. A.; Peng, Z.; Fontaine, O.; Bruce, P. G. Charging a Li–O<sub>2</sub> Battery Using a Redox Mediator. *Nat. Chem.* **2013**, *5* (6), 489–494.
- (13) Shiga, T.; Kato, Y.; Inoue, M.; Hase, Y. Bifunctional Catalytic Activity of Iodine Species for Lithium–Carbon Dioxide Battery. *ACS Sustainable Chem. Eng.* **2019**, *7* (16), 14280–14287.
- (14) Liu, T.; Leskes, M.; Yu, W.; Moore, A. J.; Zhou, L.; Bayley, P. M.; Kim, G.; Grey, C. P. Cycling Li–O<sub>2</sub> Batteries via LiOH Formation and Decomposition. *Science* **2015**, *350* (6260), 530–533.
- (15) Hou, Y.; Wang, J.; Liu, L.; Liu, Y.; Chou, S.; Shi, D.; Liu, H.; Wu, Y.; Zhang, W.; Chen, J. Mo<sub>2</sub>C/CNT: An Efficient Catalyst for Rechargeable Li–CO<sub>2</sub> Batteries. *Adv. Funct. Mater.* **2017**, *27* (27), 1700564.
- (16) King, Y.; Yang, Y.; Li, D.; Luo, M.; Chen, N.; Ye, Y.; Qian, J.; Li, L.; Yang, D.; Wu, F.; Chen, R.; Guo, S. Crumpled Ir Nanosheets Fully Covered on Porous Carbon Nanofibers for Long-Life Rechargeable Lithium–CO<sub>2</sub> Batteries. *Adv. Mater.* **2018**, *30* (51), 1803124.
- (17) Yang, S.; Qiao, Y.; He, P.; Liu, Y.; Cheng, Z.; Zhu, J.-j.; Zhou, H. A Reversible Lithium–CO<sub>2</sub> Battery with Ru Nanoparticles as a Cathode Catalyst. *Energy Environ. Sci.* **2017**, *10* (4), 972–978.
- (18) Li, S.; Liu, Y.; Zhou, J.; Hong, S.; Dong, Y.; Wang, J.; Gao, X.; Qi, P.; Han, Y.; Wang, B. Monodispersed MnO Nanoparticles in Graphene-an Interconnected N-doped 3D Carbon Framework as a Highly Efficient Gas Cathode in Li–CO<sub>2</sub> Batteries. *Energy Environ. Sci.* **2019**, *12* (3), 1046–1054.
- (19) Fuller, T. F.; Harb, J. N. *Electrochemical Engineering*; John Wiley & Sons: 2018.
- (20) Wei, S.; Choudhury, S.; Tu, Z.; Zhang, K.; Archer, L. A. Electrochemical Interphases for High-Energy Storage Using Reactive Metal Anodes. *Acc. Chem. Res.* **2018**, *51* (1), 80–88.
- (21) Öhman, L. O.; Edlund, U. Aluminum-27 NMR of Solutions. *eMagRes* **2007**, DOI: 10.1002/9780470034590.emrstm0007.
- (22) Pan, C.; Shin, M.; Liu, D.; Kottwitz, M.; Zhang, R.; Nuzzo, R. G.; Gewirth, A. A. Energy Storage Mechanisms in High-Capacity Graphitic C<sub>3</sub>N<sub>4</sub> Cathodes for Al-Ion Batteries. *J. Phys. Chem. C* **2020**, *124* (19), 10288–10297.
- (23) Zhang, M.; Kamavarum, V.; Reddy, R. G. New Electrolytes for Aluminum Production: Ionic liquids. *Jom* **2003**, *55* (11), 54–57.
- (24) Jin, C.; Liu, T.; Sheng, O.; Li, M.; Liu, T.; Yuan, Y.; Nai, J.; Ju, Z.; Zhang, W.; Liu, Y.; et al. Rejuvenating Dead Lithium Supply in Lithium Metal Anodes by Iodine Redox. *Nature Energy* **2021**, *6* (4), 378–387.
- (25) Yin, W.; Grimaud, A.; Lepoivre, F.; Yang, C.; Tarascon, J. M. Chemical vs Electrochemical Formation of Li<sub>2</sub>CO<sub>3</sub> as a Discharge Product in Li–O<sub>2</sub>/CO<sub>2</sub> Batteries by Controlling the Superoxide Intermediate. *Journal of physical chemistry letters* **2017**, *8* (1), 214–222.

## Recommended by ACS

### Fully Biodegradable and Long-Term Operational Primary Zinc Batteries as Power Sources for Electronic Medicine

Xueying Huang, Lan Yin, et al.

MARCH 10, 2023  
ACS NANO

READ

### Simultaneous Knockdown of Immune Suppressive Markers by Tumor Microenvironment-Responsive Multifaceted Prodrug Nanomedicine

Liuwei Zhang, Qixian Chen, et al.

MARCH 01, 2023  
ACS APPLIED MATERIALS & INTERFACES

READ

### Repurposing Xylan Biowastes for Sustainable Household Detergents

Hairong Wang, Feng Peng, et al.

FEBRUARY 09, 2023  
ACS SUSTAINABLE CHEMISTRY & ENGINEERING

READ

### Facile Tailoring of Surface Terminations of MXenes by Doping Nb Element: Toward Extraordinary Pseudocapacitance Performance

Jianguang Xu, Chi Chen, et al.

MARCH 16, 2023  
ACS APPLIED MATERIALS & INTERFACES

READ

Get More Suggestions >